

Size effects and depolarization field influence on the phase diagrams of cylindrical ferroelectric nanoparticles.

Anna N.Morozovska¹,

¹V. Lashkaryov Institute of Semiconductor Physics, NAS of Ukraine,
41, pr. Nauki, 03028 Kiev, Ukraine, morozo@mail.i.com.ua

Eugene A. Eliseev², Maya D.Glinchuk²

²Institute for Problems of Materials Science, NAS of Ukraine,
Krjjanovskogo 3, 03142 Kiev, Ukraine, glin@materials.kiev.ua

Abstract

Ferroelectric nanoparticles of different shape and their nanocomposites are actively studied by modern physics. Because of their applications in many fields of nanotechnology, the size effects and the possible disappearance of ferroelectricity at a critical particle volume attract a growing scientific interest. In this paper we study the size effects of the cylindrical nanoparticle phase diagrams allowing for effective surface tension and depolarization field influence. The Euler-Lagrange equations were solved by direct variational method. The approximate analytical expression for the paraelectric-ferroelectric transition temperature dependence on nanoparticle sizes, polarization gradient coefficient, extrapolation length, effective surface tension and electrostriction coefficient was derived. It was shown that the transition temperature could be higher than the one of the bulk material for nanorods and nanowires in contrast to nanodisks, where the decrease appears. We proved that among all cylindrical shapes a nanobar reveals the minimal critical volume. Therefore we predict conservation and enhancement of ferroelectric properties in nanorods and nanowires. Obtained results explain the observed ferroelectricity enhancement in nanorods and could be very useful for elaboration of modern nanocomposites with perfect polar properties.

PACS: 77.80.-e, 77.84.Dy, 68.03.Cd, 68.35.Gy

1. Introduction

Ferroelectric nanoparticles of different shape are actively studied in nano-physics and nano-technology. Because of miniaturization of devices based on these materials, the study of ferroelectric properties size dependence and the possible disappearance of ferroelectricity at a finite critical volume attract a great interest.

The ferroelectric phase was studied in ferroelectric nanowires, nanotubes and nanorods, [1], [2], [3], [4], [5]. It is appeared that nanorods and nanotubes posses such polar properties as remnant polarization [1] and piezoelectric hysteresis [4], [5], [3]. Moreover, co-called “confined” geometry does not destroy ferroelectric phase as predicted for spherical particles by [6], [7] and observed by [8], [9], [10], but sometimes the noticeable enhancement of ferroelectric properties appears in nano-cylinders [1], [2], [3], [4], [5], [11].

Yadlovker and Berger [1] reported about the spontaneous polarization enhancement about $0.25-2\mu\text{C}/\text{cm}^2$ and ferroelectric phase conservation in Roshelle salt (**RS**) nanorods (radius about 30nm and height 500nm) up to the material decomposition temperature 55°C that is about 30°C higher than the one of bulk-size crystals.

Mishina *et al* [11] revealed that ferroelectric phase exists in $\text{PbZr}_{0.52}\text{Ti}_{0.48}\text{O}_3$ (**PZT**) nanorods with diameter less than 10-20nm. However, earlier Mishra *et al* [9] demonstrated that the ceramics prepared from the powders of $\text{PbZr}_{0.52}\text{Ti}_{0.48}\text{O}_3$ with size about 100 nm had a pseudo-cubic symmetry, but might exhibit a hump in the temperature variation of dielectric constant. So, it seems that the critical size for the PZT nanorod (if any) is about 10 times smaller than the one for the nanosphere.

Geneste *et al* [2] studied the size dependence of the ferroelectric properties of BaTiO_3 (**BT**) nanowires from the first principles. They showed that the ferroelectric distortion along the wire axis disappears below a critical size of about 1.2nm, also it can be recovered under the appropriate strain conditions. Note, that BaTiO_3 spherical nanoparticles have the much longer critical diameter of about 100nm [10].

Morrison *et al* [5] demonstrated that ultra-small $\text{PbZr}_{0.52}\text{Ti}_{0.48}\text{O}_3$ nanorods and nanotubes (radius 20-30nm, length $50\mu\text{m}$) possesses rectangular shape of the piezoelectric hysteresis loop with effective remnant piezoelectric coefficient value compatible with the ones typical for PZT films [12]. This fact unambiguously speaks in favor of spontaneous polarization existence. Also the authors demonstrated that the ferroelectric properties of the free BaTiO_3 nanotubes are perfect.

Thus, at the first glance recent experimental results contradict the generally accepted viewpoint that the ferroelectric properties disappear under the system volume decreases below the critical one [13]. Actually the aforementioned facts proved that the shape of nanoparticles (e.g. the spherical or cylindrical one) essentially influences on the critical volume necessary for the ferroelectricity conservation [2] possibly owing to the different depolarization field and mechanical boundary

conditions [14], [15]. Immediately one should ask the principal question: “What nanoparticle shape posses the minimal critical volume and allows ferroelectricity conservation at higher temperatures? Could the answer be predicted theoretically?

In theoretical papers [6], [16] the special attention was paid to size effects, but depolarization electric field influence on a nanoparticle was neglected. However, it is well known that depolarization field exists in the majority of confined ferroelectric systems [17] and causes the aforementioned size-induced ferroelectricity disappearance in insulator single-domain films and ellipsoidal particles [18], [19], [20]. Both finite size and depolarization field effects lead to the ferroelectric properties degradation, namely the phase transition temperature in spherical nanoparticles is significantly lower the bulk one for most of the cases [6], [21], [20], [8].

In this paper we study the size effects, surface tension and depolarization field influence on the non-interacting nanoparticles assembly. We suppose that a nanoparticle surface is covered with a charged layer consisted of the free carriers adsorbed in the ambient conditions (e.g. air with definite humidity or pores filled with a precursor water solution). For instance a thin water layer condensates on the polar oxide surface in the air with humidity 20-50% [22]. The surface charges screen the surrounding medium from the nanoparticle electric field [13], but the depolarization field inside the particle is caused by inhomogeneous polarization distribution. Thus we calculated the depolarization field inside a cylindrical nanoparticle under the short-circuit conditions proposed by Kretschmer and Binder [18].

For the description of nanodisks, nanorods and nanowires ferroelectric properties we used the Euler-Lagrange equations solved by means of a direct variational method [19]. The approximate analytical expression for paraelectric-ferroelectric transition temperature dependence on the nanoparticle sizes, extrapolation length, effective surface tension coefficient, polarization gradient and piezoelectric coupling coefficients *etc* was derived. We obtained, that the possible reason of the polar properties enhancement in confined ferroelectric nanowires and nanorods is the converse electrostriction effect caused by the effective surface pressure.

2. Free energy with renormalized coefficients

Let us consider ferroelectric cylindrical nanoparticle with radius R , height h and polarization $P_z(\rho, z)$ oriented along z -axes. Hereinafter $V = \pi R^2 h$ is the particle volume, the polarization distribution $P_z(\rho, z)$ is axisymmetric. The external electric field is $\mathbf{E} = (0, 0, E_0)$ (see Fig. 1).

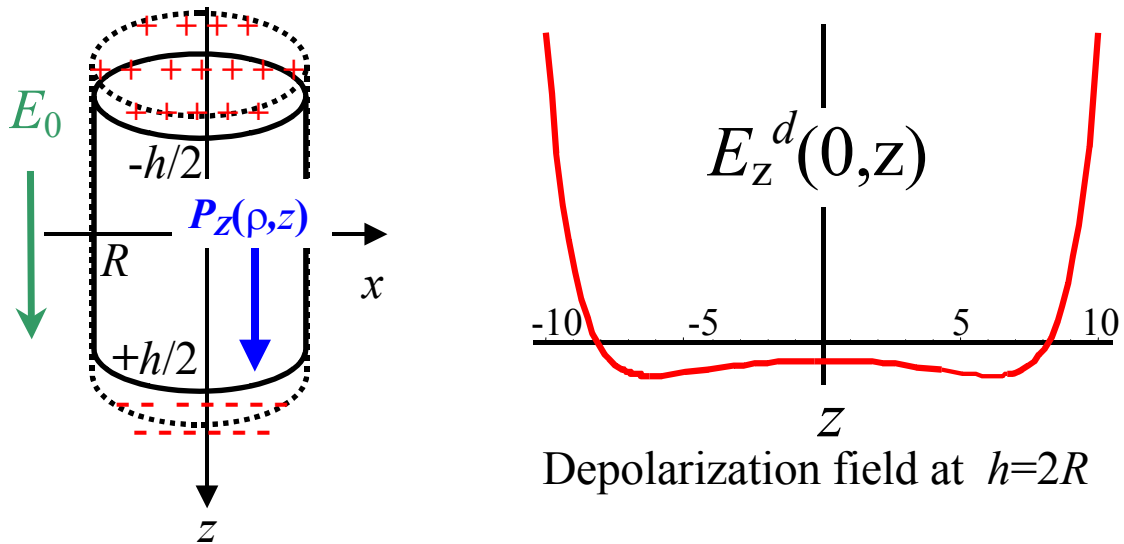


FIG. 1. (Color online) The scheme of calculation and depolarization field distribution on a nanoparticle z-axis.

The coupled equations for the polarization can be obtained by the variation on polarization of the free energy functional $\Delta G = \Delta G_V + \Delta G_S$ consisted from the bulk part ΔG_V and the surface one ΔG_S [15]. The bulk part ΔG_V acquires the form:

$$\Delta G_V = 2\pi \int_{-h/2}^{h/2} dz \int_0^R \rho d\rho \left(\frac{\alpha_R(T)}{2} P_z^2(\rho, z) + \frac{\beta_z}{4} P_z^4(\rho, z) + \frac{\gamma_z}{6} P_z^6(\rho, z) + \frac{\delta}{2} (\nabla P_z(\rho, z))^2 - P_z(\rho, z) \left(E_0 + \frac{E_z^d(\rho, z)}{2} \right) \right) \quad (1)$$

Material coefficients $\delta > 0$, while $\beta < 0$ for the first order phase transitions or $\beta > 0$ for the second order ones. The coefficient $\alpha_R(T)$ in Eq.(1) should be renormalized by the external stress (see e.g. Ref. [21], [23]). In Appendix A we study the influence of the effective surface tension on a cylindrical particle and derived the expression for $\alpha_R(T)$:

$$\alpha_R(T, R) = \alpha_T(T - T_C) + 2Q_{12} \frac{\mu}{R} \quad . \quad (2)$$

Here parameters T_C , α_T and Q_{12} are respectively Curie temperature, inverse Curie constant, and electrostriction coefficient regarded known for the bulk material. The parameter μ is the effective surface tension coefficient between the nanoparticle and interface [24], [10].

It should be noted that Huang *et al.* [21] proposed the model in which the surface bond contraction induces a compressive stress $p \sim 1/R^2$ inside a spherical particle. Note, that the renormalization of coefficient $\alpha_R = \alpha + 2Q_{12}p$ for a cylindrical nanoparticle differs from the one $\alpha_R = \alpha + (Q_{11} + 2Q_{12})p$ obtained by [21]. Both results are clear owing to the fact that stresses $\sigma_1 = \sigma_2 = -p$ and $\sigma_3 = 0$ for a cylinder, whereas $\sigma_1 = \sigma_2 = \sigma_3 = -p$ for a sphere. Also we do not

take into account possible stress relaxation caused by dislocations. This approach used by many authors is valid for the small enough particle radius [25].

The depolarization electric field inside the finite cylindrical nanoparticle cannot be derived in the similar way as the field of the spherical one, because a finite cylinder is not a spheroid. The exact expression for depolarization field $\mathbf{E}^d(\rho, z)$ inside the cylindrical nanoparticle covered with screening charges is derived in Appendix B (see Eq.(B.6)). Hereinafter we use its Pade approximation:

$$\left\{ \begin{array}{l} E_Z^d(\rho, z) \approx \eta(R, h) \cdot (\langle P_Z \rangle - P_Z(\rho, z)), \\ \eta(R, h) = \frac{4\pi}{1 + (h/2R)^2} \end{array} \right. \quad (3)$$

The angular brackets are the spatial averaging on the particle volume V , e.g. $\langle P_Z \rangle \equiv \frac{2\pi}{V} \int_{-h/2}^{h/2} dz \int_0^R \rho d\rho P_Z(\rho, z)$. The function $\eta \sim (2R/h)^2 \ll 1$ for the prolate cylinder with $R \ll h$ [17], whereas $\eta \rightarrow 4\pi$ for the oblate cylinder with $R \gg h$ [18]. It should be noted that the depolarization field is absent outside the particles in the framework of our model. Therefore the interaction of such nanoparticles is practically absent due to the screening. Their composite can be considered as the assembly of independent particles.

The surface part of the polarization-dependent free energy ΔG_s is supposed proportional to square of polarization on the particle surface S , namely $\Delta G_s = \frac{\delta}{2} \int_S \frac{ds}{\lambda} P_s^2$ (λ is the extrapolation length [6], [16]). A cylindrical nanoparticle has upper and bottom surfaces $z = h/2$, $z = -h/2$ and a sidewall $\rho = R$, so its surface energy ΔG_s acquires the form:

$$\Delta G_s = \delta \left(\int_0^R \frac{2\pi\rho}{\lambda_b} d\rho \left(P_Z^2 \left(\rho, z = \frac{h}{2} \right) + P_Z^2 \left(\rho, z = -\frac{h}{2} \right) \right) + \int_{-h/2}^{h/2} \frac{2\pi R dz}{\lambda_s} P_Z^2(\rho = R, z) \right). \quad (4)$$

We introduced longitudinal and lateral extrapolation lengths $\lambda_b \neq \lambda_s$ in Eq.(4). Hereinafter we regard these extrapolation lengths positive.

Variation of the free energy expressions (1) + (4) yields the following Euler-Lagrange equations with the boundary conditions on the cylinder butts $z = \pm h/2$ [19], and the sidewall surface $\rho = R$ [6]:

$$\left\{ \begin{array}{l} \alpha_R P_Z(\rho, z) + \beta P_Z^3(\rho, z) + \gamma P_Z^5(\rho, z) - \delta \left(\frac{\partial^2 P_Z(\rho, z)}{\partial z^2} + \frac{1}{\rho} \frac{\partial}{\partial \rho} \rho \frac{\partial}{\partial \rho} P_Z(\rho, z) \right) = E_0 + E_Z^d(\rho, z), \\ \left(P_Z + \lambda_b \frac{dP_Z}{dz} \right) \Big|_{z=h/2} = 0, \quad \left(P_Z - \lambda_b \frac{dP_Z}{dz} \right) \Big|_{z=-h/2} = 0, \quad \left(P_Z + \lambda_s \frac{dP_Z}{d\rho} \right) \Big|_{\rho=R} = 0, \end{array} \right. \quad (5)$$

Let us find the approximate solution of the nonlinear Eq.(5) by using the direct variational method as proposed in [19]. Firstly we solved the linearized Eq.(5):

$$P_z(\rho, z) = \sum_{n=1}^{\infty} \frac{2J_0(k_n \rho / R)}{k_n J_1(k_n)} \left(\frac{E_0 + \eta \langle P_z \rangle}{\alpha_R + \eta + \delta(k_n / R)^2} (1 - \varphi_n(z)) \right) \quad (6)$$

$$\varphi_n(z) = \frac{ch(\xi_n z)}{ch(\xi_n h/2) + \lambda_b \xi_n sh(\xi_n h/2)}, \quad \begin{cases} \xi_n = \sqrt{(k_n / R)^2 + (\alpha_R + \eta) / \delta} \\ J_0(k_n) - (\lambda_s / R) k_n J_1(k_n) = 0 \end{cases} \quad (7)$$

Here $J_0(k_n)$ and $J_1(k_n)$ are Bessel functions of the zero and first orders respectively. In general case the roots k_n depend over the ratio (λ_s / R) in accordance with Eq.(7). Under the condition $(\lambda_s / R) \ll 1$ one obtains that $J_0(k_n) \approx 0$. For the case we used the Bessel functions norm $\langle J_0(k_n \rho / R) J_0(k_m \rho / R) \rangle = \delta_{nm} J_1^2(k_n)$ and equality $\langle J_0(k_m \rho / R) \rangle = 2J_1(k_m) / k_m$ in Eq.(7) [26].

The average paraelectric polarization and dielectric permittivity acquire the form:

$$\langle P_z \rangle = \frac{\sum_{n=1}^{\infty} \frac{4}{k_n^2} \left(\frac{E_0 (1 - \Phi_n)}{\alpha_R + \eta + \delta(k_n / R)^2} \right)}{1 - \eta \sum_{n=1}^{\infty} \left(\frac{4}{k_n^2} \cdot \frac{1 - \Phi_n}{\alpha_R + \eta + \delta(k_n / R)^2} \right)}, \quad (8)$$

$$\langle \epsilon_{zz} \rangle = \frac{d \langle P_z \rangle}{d E_0} = \frac{4\pi \sum_{n=1}^{\infty} \frac{4}{k_n^2} \frac{(1 - \Phi_n)}{\alpha_R + \eta + \delta(k_n / R)^2}}{1 - \eta \sum_{n=1}^{\infty} \left(\frac{4}{k_n^2} \cdot \frac{1 - \Phi_n}{\alpha_R + \eta + \delta(k_n / R)^2} \right)}. \quad (9)$$

Hereinafter $\langle \varphi_n(z) \rangle \equiv \Phi_n = \frac{2}{\xi_n h} \cdot \frac{sh(\xi_n h/2)}{ch(\xi_n h/2) + \lambda_b \xi_n sh(\xi_n h/2)}$.

Note, that the expression for paraelectric permittivity $\langle \epsilon_{zz} \rangle$ obtained from Eq.(9) coincides with one derived by Wang *et. al* [6] for the infinite cylinder at $(\lambda_s / R) \rightarrow 0$. In fact, for the case of infinite cylinder ($h \rightarrow \infty$) one can neglect the depolarization field ($\eta \rightarrow 0$) and dependence on z ($\varphi_n(z) \rightarrow 0$), so the summation on k_n leads to

$$P_z(\rho, h \rightarrow \infty) = E_0 \sum_{n=1}^{\infty} \frac{2J_0(k_n \rho / R)}{k_n J_1(k_n)} \frac{1}{\alpha_R + \delta(k_n / R)^2} \equiv \frac{E_0}{-\alpha_R} \left(\frac{J_0(\rho \sqrt{-\alpha_R / \delta})}{J_0(R \sqrt{-\alpha_R / \delta})} - 1 \right), \quad (10)$$

$$\langle P_z \rangle = E_0 \sum_{n=1}^{\infty} \frac{4}{k_n^2} \frac{1}{\alpha_R + \delta(k_n / R)^2} \equiv \frac{E_0}{\alpha_R} \left(1 - \frac{2}{R \sqrt{-\alpha_R / \delta}} \frac{J_1(R \sqrt{-\alpha_R / \delta})}{J_0(R \sqrt{-\alpha_R / \delta})} \right).$$

In order to obtain the free energy with renormalized coefficients, let us use the coordinate-dependent part of the obtained solution in the trial function $P_z(\rho, z) = \sum_{n=1}^{\infty} \frac{2J_0(k_n \rho / R)}{k_n J_1(k_n)} \frac{1 - \Phi_n(z)}{1 - \Phi_n} P_n$.

The variation amplitudes P_n must be determined by the minimization of the expressions (1)-(4). Integration in these expressions with the aforementioned trial function leads to the following form of the free energy:

$$\begin{aligned} \Delta G = & \frac{1}{2} \sum_{n=1}^{\infty} \frac{\alpha_R + \eta + \delta(k_n / R)^2}{1 - \Phi_n} \frac{4P_n^2}{k_n^2} - \frac{\eta}{2} \left(\sum_{n=1}^{\infty} \frac{4P_n}{k_n^2} \right)^2 - E_0 \sum_{n=1}^{\infty} \frac{4P_n}{k_n^2} + \\ & + \frac{\beta}{4} \left(\sum_{l,n,s,q} g_{lnsq} P_l P_n P_s P_q \right) + \frac{\gamma}{6} \left(\sum_{l,n,s,q,r,t} f_{lnsqr} P_l P_n P_s P_q P_r P_t \right) \end{aligned} \quad (11)$$

The exact expressions for the renormalized coefficients in Eq.(11) are rather cumbersome. Note, that hereinafter we suppose that $\xi_n^2 \lambda_b h \gg 1$ and so $\Phi_n \approx 2/h \xi_n (1 + \lambda_b \xi_n) \ll 1$, which is typical for the majority of ferroelectric nanoparticles. Really, using typical values $|\alpha| = 10^{-2}$, $\delta = 10^{-19} m^2$ and $\lambda_b = 10^{-8} m$, one can easily obtain that $\xi_n^2 \approx 4\pi/\delta$ and so $\xi_n^2 \lambda_b h \sim 10^2 - 10^3$ for disks of radius $R \gg h \sim 10^{-9} m$, whereas $\xi_n^2 \approx (k_n / R)^2 + \alpha/\delta \sim 10^{18} m^{-2}$ and thus $\xi_n^2 \lambda_b h \sim 10^1 - 10^2$ for wires of length $h \gg R \sim 10^{-9} m$.

The average polarization should be calculated as:

$$\langle P_z \rangle = \sum_{n=1}^{\infty} \frac{4P_n}{k_n^2}, \quad (12)$$

The coupled equations for the amplitudes P_n should be obtained from the variation $\frac{\partial \Delta G}{\partial P_n} = 0$.

Note, that Yadlovker and Berger [1] observed ferroelectric domains with walls oriented along the rod polar axis in a nanoparticle of RS. Keeping in mind, that the domain wall energy are represented by the correlation term $\frac{\delta}{2} (\nabla P_z(\rho, z))^2$ in Eq.(1) for the continuous media approximation, polydomain states could be studied with the help of the free energy (1)-(4). However, for these states adequate description one should use exact expression (B.6) for the depolarization field and calculate the polarization distribution $P_z(\rho, z) = \sum_{m=0}^{\infty} \sum_{n=1}^{\infty} P_{mn} \cos\left(\frac{2\pi m}{h} z\right) J_0\left(k_n \frac{\rho}{R}\right)$ in accordance with Eqs. (B.7), (B.6) and (5) self-consistently. The contour lines of depolarization field isopotential lines and spontaneous polarization spatial distribution for a single- and poly-domain states of the nanorod with $R = 2h$ are depicted in Fig. 2. (MD, probably this item should be removed ...)

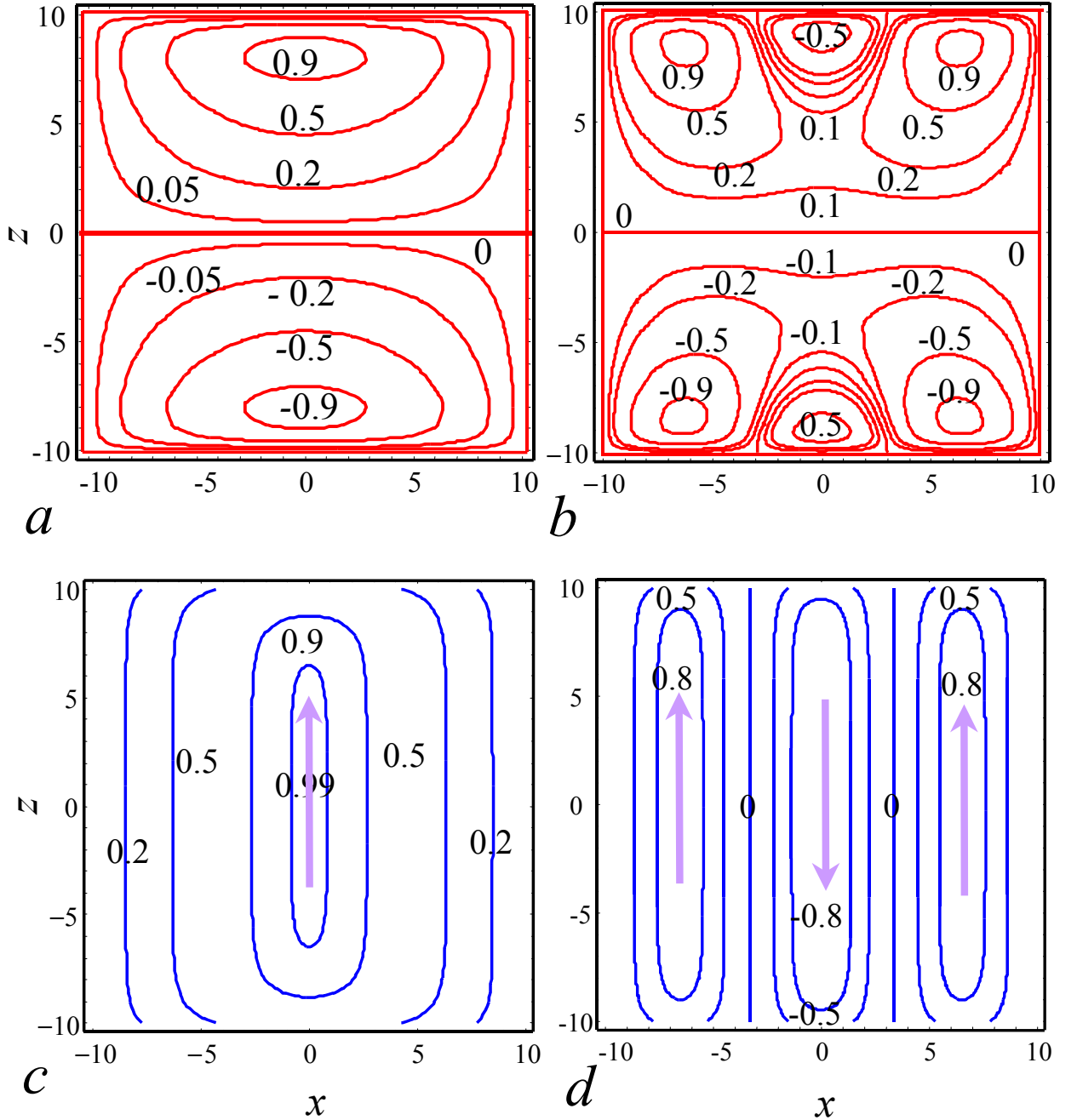


FIG. 2. (Color online) Depolarization field isopotential lines (a, b) and contour lines of spontaneous polarization spatial distribution (c, d) for a single- (a, c) and poly-domain states (b, d) of the nanorod with $h = 2R$. Numbers near curves correspond to the values of polarization and potential normalized on their maximal values.

3. Phase diagram

The equation for paraelectric-ferroelectric phase transition temperature $T_{CN}(R, h)$ can be obtained from Eq. (9) in the following form:

$$1 - \eta(R, h) \sum_{n=1}^{\infty} \frac{4}{k_n^2} \frac{1 - \Phi_n(R, h, T_{CN})}{\alpha_R(T_{CN}) + \eta(R, h) + \delta(k_n/R)^2} = 0. \quad (13)$$

In particular case $\xi_n^2 \lambda_b h \gg 1$ we derived the interpolation for $T_{CN}(R, h)$ valid for the nanodisks, nanorods and nanowires:

$$T_{CN}(R, h) \approx T_C \left(1 - \frac{2\mu Q_{12}}{\alpha_T T_C R} - \frac{k_1^2 \delta}{\alpha_T T_C R^2} - \frac{2\eta(R, h)}{\alpha_T T_C (1 + \lambda_b \xi) \xi h} \right), \quad (14)$$

where $\xi(R, h) = \sqrt{\frac{1}{\delta} \left(\frac{k_1^2 \delta}{R^2} + \eta(R, h) \right)}$, $k_1 \approx 2.405$.

The first term in Eq.(14) is the bulk transition temperature, the second term is related to the electrostriction effect via surface pressure, the third one corresponds to the correlation effects, and the fourth represents the depolarization field contribution. The depolarization field is small enough at $h \gg R$. The correlation and depolarization terms are always negative and thus only decrease the transition temperature, whereas the second electrostriction term $\frac{2\mu Q_{12}}{\alpha_T T_C R}$ in Eq. (14) could be positive or negative depending on the Q_{12} sign. Note, that both signs of Q_{12} are possible for different ferroelectrics, however $Q_{12} < 0$ and $Q_{11} + 2Q_{12} > 0$ for most of the perovskite ferroelectrics. Below we demonstrate that increasing of transition temperature and thus ferroelectric properties enhancement and conservation is possible when $\frac{2\mu Q_{12}}{\alpha_T T_C R} < 0$ and depolarization field is small enough. The latter is impossible for the spherical particles with positive renormalization $(Q_{11} + 2Q_{12})\mu > 0$ [21].

Let us make some estimation of the second and third terms in Eq.(14) for perovskites BaTiO₃ and PbTiO₃. Using parameters $Q_{12} = -0.043 \text{ m}^4 / \text{C}^2$, $T_C = 400 \text{ K}$ (BaTiO₃) and $Q_{12} = -0.046 \text{ m}^4 / \text{C}^2$, $T_C = 666 \text{ K}$ (PbZr_{0.5}Ti_{0.5}O₃) and $\mu = 5 - 50 \text{ N/m}$ [10], $\delta = 10^{-19} \text{ m}^2$, we obtained that $\left| \frac{2\mu Q_{12}}{\alpha_T T_C} \right| \approx 2 - 17 \text{ nm}$, $\sqrt{\frac{\delta k_1^2}{\alpha_T T_C}} \approx 5 \text{ nm}$ for BaTiO₃ and $\left| \frac{2\mu Q_{12}}{\alpha_T T_C} \right| \approx 3 - 26 \text{ nm}$, $\sqrt{\frac{\delta k_1^2}{\alpha_T T_C}} \approx 5 \text{ nm}$ for PbZr_{0.5}Ti_{0.5}O₃ respectively. So both terms are comparable with unity at nanoparticle radius $\sim 2-25 \text{ nm}$.

For a **bulk sample** $R \rightarrow \infty$, $h \rightarrow \infty$ and one obtains that $T_{CN}(R, h) \rightarrow T_C$ as it should be expected. For a **nanodisk** with $R \gg h$ values $\eta \rightarrow 4\pi$ and $\xi_n \rightarrow \sqrt{4\pi/\delta}$, so the renormalized transition temperature acquires the form similar to the one derived in [20]. For a **nanowire** with $h \rightarrow \infty$ values $\eta \rightarrow 0$ and $\langle \phi(\xi_n) \rangle \sim 1/\xi_n h \rightarrow 0$, i.e. the depolarization field vanishes, thus $T_{CN}(R, h) \approx T_C - \frac{2\mu Q_{12}}{\alpha_T R} - \frac{k_1^2 \delta}{\alpha_T R^2}$. Intermediate situation is realized in prolate **nanorods**, when the

inequality $h \gg R$ is valid, but the small values $\langle \phi(\xi_n) \rangle \approx \frac{2}{(1 + \lambda_b \xi_n) \xi_n h}$ and $\eta(R, h) \approx 16\pi \cdot \frac{R^2}{h^2}$ are non-zero.

Below we present phase diagrams and polar properties calculations based on the Eqs (13)-(14). Our calculations are presented in the Figs. 3-5. Taking into account that $\sqrt{\delta} \sim 0.5 \text{ nm}$ is of a lattice constant order, we introduced the following parameters and dimensionless variables:

$$R_\mu = \frac{2\mu Q_{12}}{\alpha_T T_C \sqrt{\delta}}, \quad R_s = \sqrt{\frac{k_1^2}{\alpha_T T_C}}, \quad r = \frac{R}{\sqrt{\delta}}, \quad l = \frac{h}{\sqrt{\delta}}, \quad \Lambda_b = \frac{\lambda_b}{\sqrt{\delta}}, \quad \Lambda_s = \frac{\lambda_s}{\sqrt{\delta}}. \quad (15)$$

In these variables

$$\begin{cases} T_{CN}(r, l) \approx T_C \left(1 - \frac{R_\mu}{r} - \frac{R_s^2}{r^2} - \frac{2\eta(r, l)}{\alpha_T T_C (1 + \Lambda_b \zeta(r, l)) \zeta(r, l) l} \right), \\ \zeta(r, l) = \sqrt{\left(\frac{k_1^2}{r^2} + \eta(r, l) \right)}, \quad k_1 \approx 2.405. \end{cases} \quad (16)$$

The **critical sizes** can be found from the equation $T_{CN}(r, l) = 0$, i.e. dependence $l_{cr}(r)$ determines the boundary between the paraelectric and ferroelectric phase (see and bold solid curve in the Fig. 3).

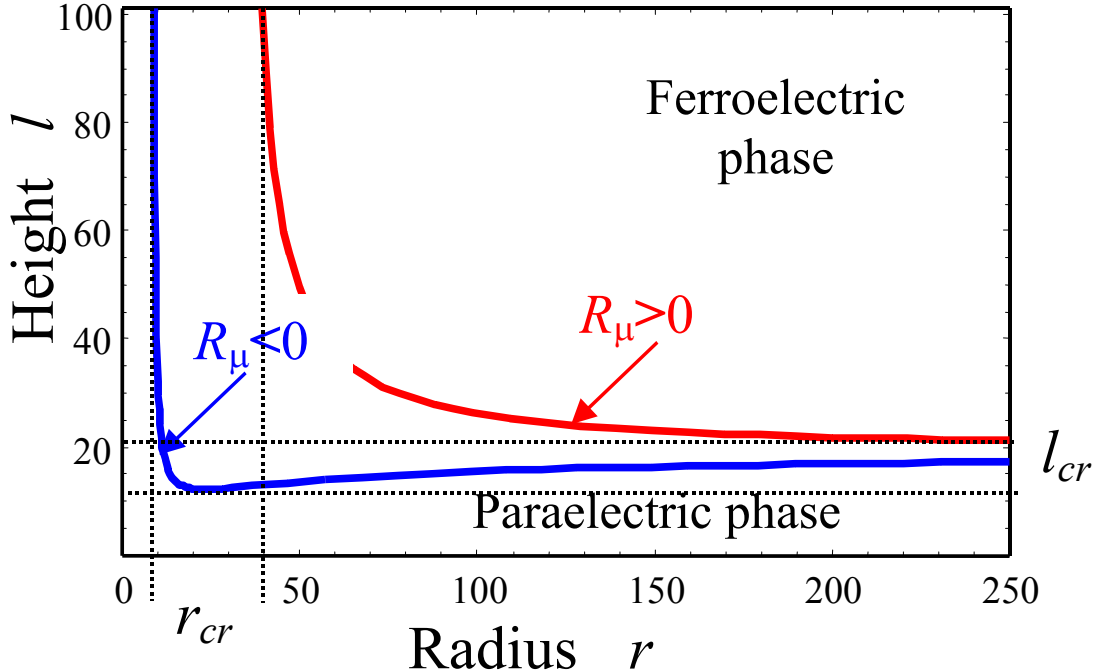


FIG. 3. (Color online) Cylindrical nanoparticles phase diagram. Parameters: $\alpha_T T_C = 3 \cdot 10^{-2}$, $\Lambda_s \leq 1$ and $\Lambda_b = 5$, $R_\mu = \pm 25$, $R_s = 17$. In Figs. 2-4 material parameters correspond to $\text{PbZr}_{0.5}\text{Ti}_{0.5}\text{O}_3$.

It is clear that ferroelectric phase appreciably broadens at $R_\mu < 0$ in comparison with the one at $R_\mu > 0$. In fact, at chosen material parameters ferroelectric phase is absent in the nanorods with thickness $l \leq 22$ ($R_\mu = +25$) or $l \leq 12$ ($R_\mu = -25$) owing to thickness-induced transition to paraelectric phase caused by depolarization effects (see horizontal dotted lines in the Fig. 3). On the other hand ferroelectric phase is absent in the nanorods with radius $r \leq 40$ ($R_\mu = +25$) or $r \leq 8$ ($R_\mu = -25$) owing to thickness-induced transition to paraelectric phase caused by lateral correlation effects (see vertical dotted lines in the Fig. 3).

The cases when the shape of nanoparticle is fixed ($l/2r = \text{const}$), but its radius r or length l increases are represented in the Figs. 4a, 4b respectively. It is clear from the figure that nanowires ($l/2r \geq 100$), nanorods ($l/2r \geq 10$), nanobars $l/2r \approx 1$ and nanodisks $l/2r \leq 0.1$ transition temperature values are different. The transition temperature tends to unity at $r \rightarrow \infty$ and $l \rightarrow \infty$ for any shape, as it should be expected for the bulk ferroelectric material.

It is clear from Fig. 4a that the transition temperature $T_{CN}(r)$ between the paraelectric and ferroelectric phase increases with nanoparticle radius increasing. Also the transition temperature $T_{CN}(r)$ decreases with the ratio $l/2r$ decrease: it is the highest for the nanowire, where depolarization field is absent ($\eta \rightarrow 0$ for $l \rightarrow \infty$), and only the transverse correlation effect and surface tension determine the size dependence of paraelectric-ferroelectric phase transition, then it is also the same for the nanorods with $l/2r \geq 10$ and small depolarization factors $\eta \sim (r/l)^2$. $T_{CN}(r)$ is the lowest for the nanodisks with $l/2r = 0.01$ and maximum depolarization factor $\eta \approx 4\pi$. Fig. 4b demonstrates that the transition temperature $T_{CN}(l)$ decreases with the ratio $l/2r$ increase only for $R_\mu > 0$.

Note, that nanorods have the smallest critical radius $r_{cr} \approx 8$ at $R_\mu = -25$ (compare with infinite nanowires without depolarization field). The situation is vice versa for nanodisks: they have the smallest critical length $l_{cr} \approx 20$ and the highest critical radius $r_{cr} \approx 100 - 1000$ (compare with a film at $R \rightarrow \infty$). No transition temperature increase $T_{CN}(r) > T_C$ was obtained for nanodisks; the increase exists for nanobar and nanorods only.

Finally, let us answer the main question: “What nanoparticle shape posses the minimal **critical volume** and allows ferroelectricity conservation at higher temperatures?” The case when the shape of nanoparticle is fixed ($l/2r = \text{const}$), but its volume $\pi r^2 l$ increases, is represented in the Fig. 5. It is follows from the Fig. 5 that the nanobar ($l/2r = 1$, depolarization factor $\eta \approx 2\pi$) has the smallest critical volume both at $R_\mu > 0$ and at $R_\mu < 0$. Its ferroelectric-paraelectric transition temperature is high enough. Moreover, at $R_\mu \sim Q_{12}\mu < 0$ this shape is preferable in comparison with a spherical one,

because a sphere has positive parameter $R_\mu \sim (Q_{11} + 2Q_{12})\mu$ and only slightly smaller depolarization factor $\eta = 4\pi/3$ [20]. The nanorod with the shape $1 < l/2r \leq 10$ reveals the highest transition temperature and thus the best ferroelectric properties at $R_\mu < 0$.

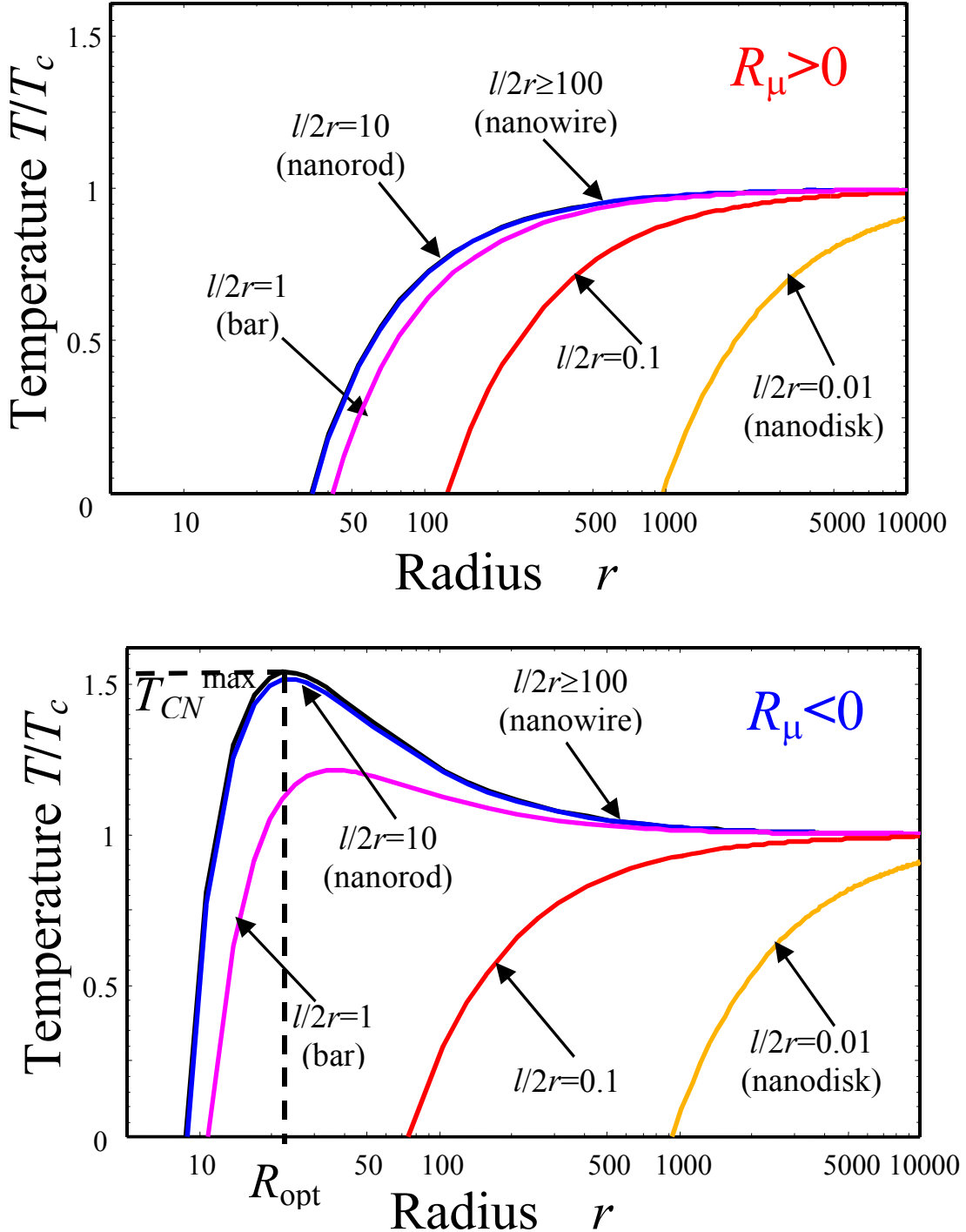


FIG. 4a. (Color online) Transition temperature size dependence for different ratios $l/2r = 100, 10, 1, 0.1, 0.01$. Other parameters: $\alpha_T T_C = 2.8 \cdot 10^{-2}$, $\Lambda_S \leq 1$, $R_\mu = \pm 25$, $R_S = 17$, $\Lambda_b = 5$.

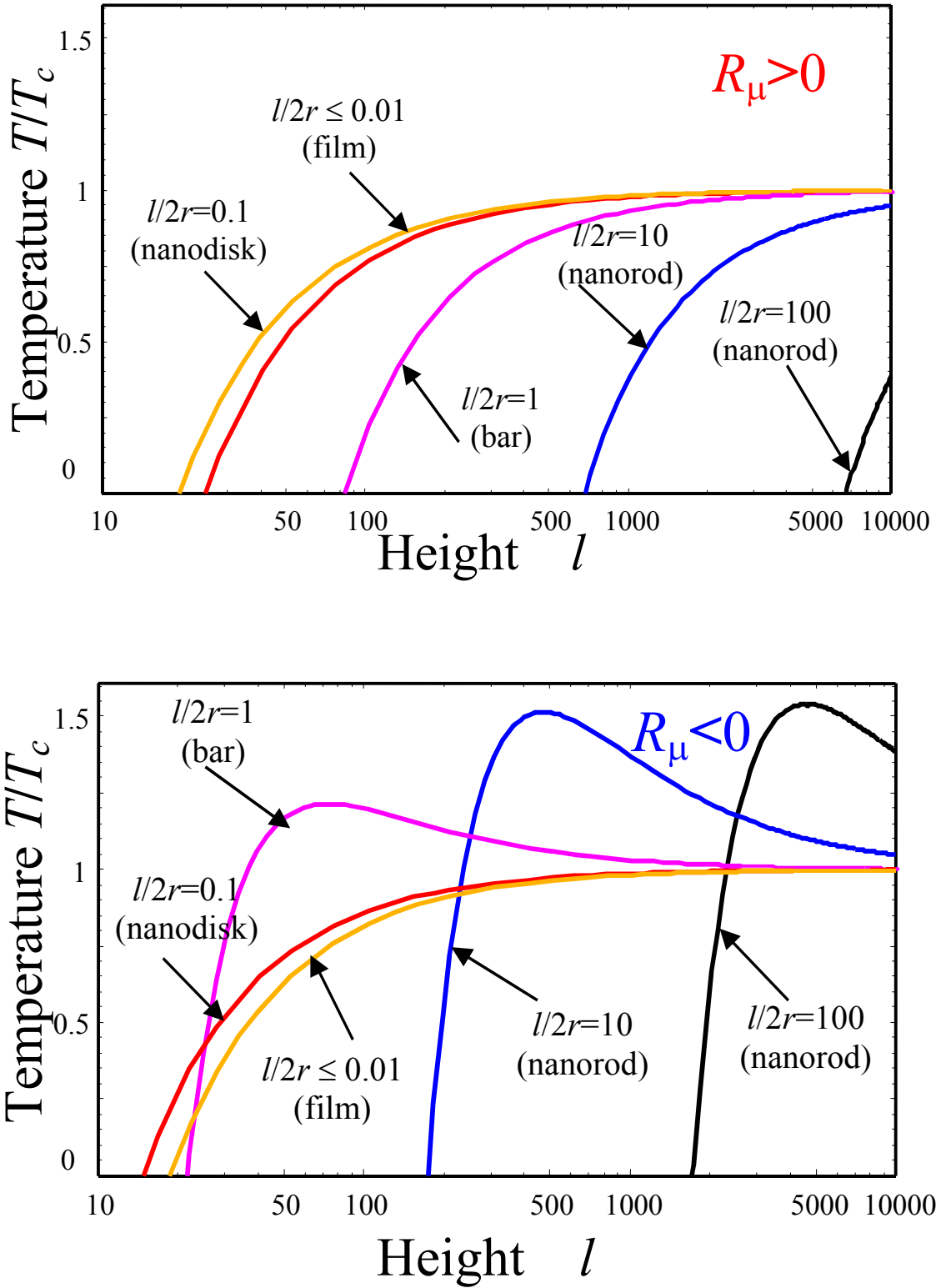


FIG. 4b. (Color online) Transition temperature size dependence for different ratios $l/2r = 100, 10, 1, 0.1, 0.01$. Other parameters: $\alpha_T T_C = 2.8 \cdot 10^{-2}$, $\Lambda_S \leq 1$, $R_\mu = \pm 25$, $R_S = 17$, $\Lambda_b = 5$.

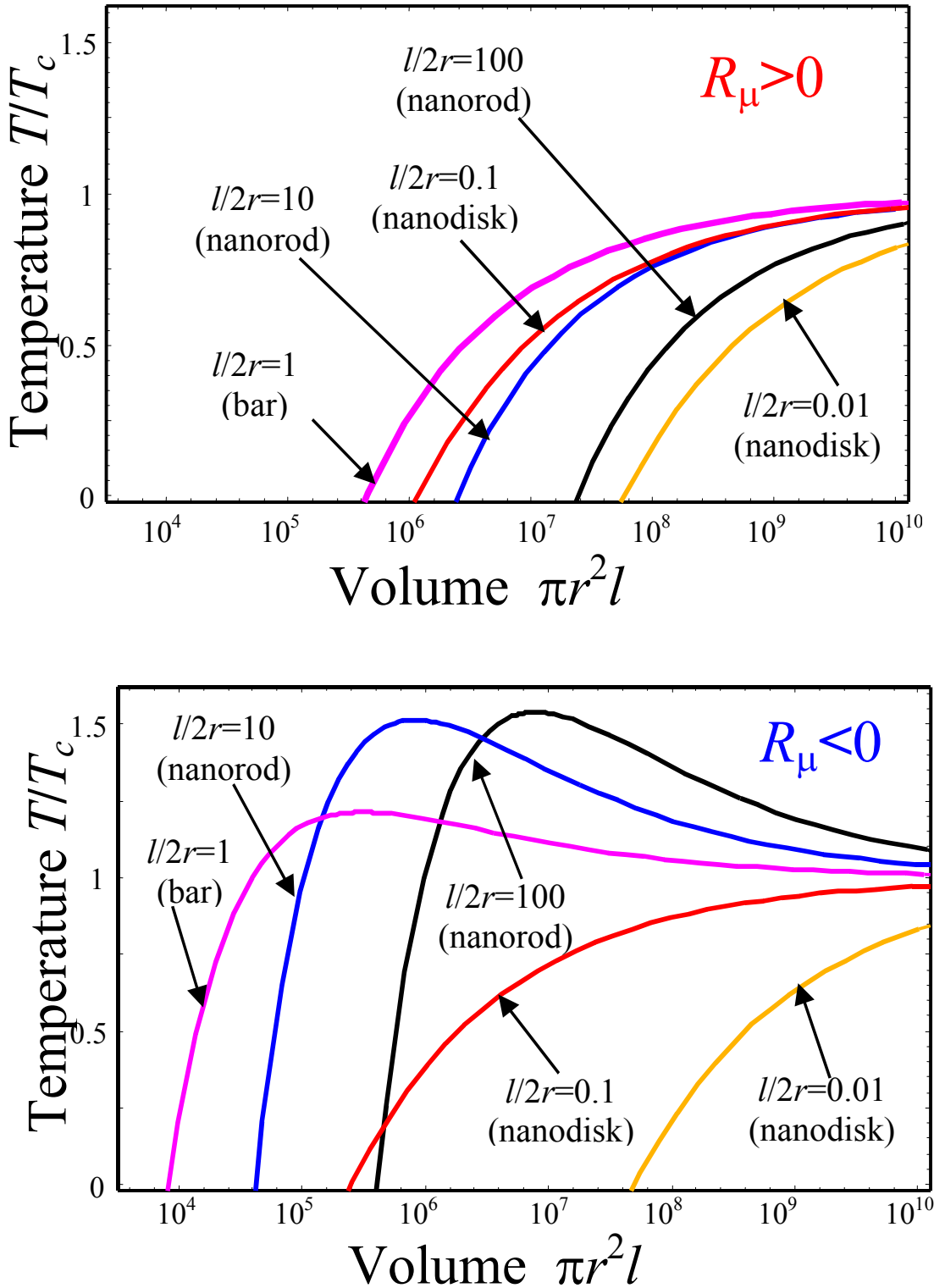


FIG. 5. (Color online) Transition temperature vs. particle volume for different ratios $l/2r = 100, 10, 1, 0.1, 0.01$. Other parameters: $\alpha_T T_c = 2.8 \cdot 10^{-2}$, $\Lambda_s \leq 1$, $R_\mu = \pm 25$, $R_s = 17$, $\Lambda_b = 5$.

In fact, the dependence of transition temperature on the nanoparticle volume is non-monotonic with respect to the ratio $l/2r$ in contrast to the monotonic radius dependencies (compare Fig. 5 with

the Figs. 4a). Thus we can conclude, that under the condition $R_\mu < 0$ nanobars and prolate nanorods ($1 \leq l/2r \leq 10$) posses enhanced polar properties at $r \sim (10 - 200)$ unit cells, namely they have higher spontaneous polarization and transition temperature in comparison with a bulk sample, whereas the **nanobar** reveals the **minimal critical volume**.

4. Discussion

Let us qualitatively compare our results with the ones obtained by [1], [11] and [2] (see Table 1).

Table 1

	Experiment or <i>ab initio</i> calculations			Proposed model						
				Critical parameters			Material constants			
Material	h , nm	R_{cr} , nm	T_{cr} , K	R_{cr} , nm	R_{opt} , nm	T_{CN}^{\max} , K	T_C, K	Q_{12} , m^4/C^2	$\delta, 10^{-19}$ m^2	$\mu, N/m$
PZT 50/50	$>>R$	5-10	300	1.1-5.3 at 300 K	2-23	704-melt	665.7	- 0.046	1	50-5
BT	$>>R$	1.2	0	1.1-3.8 at 0 K	2-24	414-melt	400	- 0.043	1	50-5
RS ^[27]	500	≤ 30	328	11-24 at 300 K	33	300-melt	297	$Q_{12}=1.56$ $Q_{13}=-2.19$	10	5-0.5

The applicability of our model to the description of phase transition between cubic paraelectric and tetragonal ferroelectric phases in BT and PZT is for certain. However, RS is known to be improper ferroelastic – ferroelectric, therefore our consideration can be applied to experiments of [1] only in the temperature range where RS ferroelectric properties can be described by the phenomenological expansion (1) over polarization powers. Moreover, we neglected the piezoelectric effect with respect to the shear stress in the paraelectric phase of RS since the effective surface tension creates no tangential stresses.

Keeping in mind that the condition $R/h \ll 1$ leads to the small values of depolarization field $E_z^d \sim \eta(R, h) \sim R^2/h^2$, the aforementioned conservation of ferroelectric properties is possible for a sufficiently “long” rod ($h/2R \geq 10$) of radius $R \sim 2 - 20$ nm. In the case we obtained, that the increase of $T_{CN}^{\max}(R_{opt}) = T_C \left(1 + \frac{R_\mu^2}{4R_s^2} \right)$ appears at radius $R_{opt} = -\frac{2R_s^2}{R_\mu}$ when the parameter $R_\mu \sim Q_{12} \mu$ is negative (see the second term in Eq.(14) and Fig. 4b), i.e. when the effective surface pressure leads to the decrease of dielectric compliance due to the negative converse electrostriction effect.

This fact has the following microscopic explanation. If the uniform lateral pressure $p = \mu/R$ via electrostriction leads to the dielectric permittivity increase in paraelectric phase, the frequency of transversal soft mode $\omega_0(T)$ decreases in accordance with the Lyddane-Sachs-Teller's relationship [28]. Taking into account that $\omega_0^2(T) \sim \epsilon_{zz}^{-1}(T) \sim |\alpha_R(T)| \sim |T - T_{CN}|$ the transition temperature T_{CN} increases. Therefore the ferroelectric instability develops at higher temperatures and polar properties are improved.

Summary

We have studied the dependence of ferroelectric nanorod **critical sizes** on the nanoparticle shape, polarization gradient coefficient, extrapolation length, effective surface tension and electrostriction coefficient Q_{12} . Analyzing obtained results we could summarize that finite nanorods of radius $R \sim 20$ - 200 unit cells posses the best ferroelectric properties when the electrostriction coefficient Q_{12} is negative, namely they exhibit the higher transition temperature and spontaneous polarization in comparison with the bulk sample, whereas a nanobar ($h/2R = 1$) reveals the **minimal critical volume**.

Obtained results explain ferroelectricity enhancement in the Rochelle salt nanorods of radius $\sim 30\text{ nm}$ [1], piezoelectric properties conservation in lead-zirconate-titanate nanorods of radius $\sim 5 - 10\text{ nm}$ [11] and are in a good agreement with the first principles calculations in barium titanate nanowires [2]. The predicted effects could be very useful for elaboration of modern nanocomposites with perfect polar properties.

References

- [1] D. Yadlovker and S. Berger, Phys. Rev. B **71**, 184112 (2005).
- [2] G. Geneste, E. Bousquest, J. Junquera, and P. Chosez, cond-mat/0503362 (unpublished).
- [3] Y. Luo, I. Szafraniak, N. D. Zakharov, V. Nagarajan, M. Steinhart, R. B. Wehrspohn, J. H. Wendroff, R. Ramesh, M. Alexe, Appl. Phys. Lett. **83**, 440 (2003).
- [4] F. D. Morrison, L. Ramsay, and J. F. Scott, J. Phys.: Condens. Matter **15**, L527 (2003).
- [5] F. D. Morrison, Y. Luo, I. Szafraniak, V. Nagarajan, R. B. Wehrspohn, M. Steinhart, J. H. Wendroff, N. D. Zakharov, E. D. Mishina, K. A. Vorotilov, A. S. Sigov, S. Nakabayashi, M. Alexe, R. Ramesh, and J. F. Scott, cond-mat/0303609 (unpublished).
- [6] C. L. Wang and S. R. P. Smith, J. Phys.: Condens. Matter **7**, 7163 (1995).
- [7] I. Rychetsky and O. Hudak, J. Phys.: Condens. Matter **9**, 4955 (1997).
- [8] D. D. Fong, G. B. Stephenson, S. K. Streiffer, J. A. Eastman, O. Auciello, P. H. Fuoss, and C. Thompson. Science **304**, 1650 (2004).
- [9] S. K. Mishra and D. Pandey. J. Phys.: Condens. Matter **7**, 9287 (1995)
- [10] K. Uchino, E. Sadanaga, and T. Hirose, J. Am. Ceram. Soc. **72**, 1555 (1989).

- [11] E. D. Mishina, K. A. Vorotilov, V. A. Vasiliev, A. S. Sigov, N. Ota, and S. Nakabayashi, *J. Exp. Theor. Phys.* **122**, 582 (2002).
- [12] B. Jaffe, W. R. Cook and H. Jaffe, *Piezoelectric Ceramics* (Academic Press, London and New York, 1971).
- [13] M. E. Lines and A. M. Glass, *Principles and Applications of Ferroelectrics and Related Phenomena* (Clarendon Press, Oxford, 1977).
- [14] N. A. Pertsev, A. G. Zembilgotov, and A. K. Tagantsev, *Phys. Rev. Lett.* **80**, 1988 (1998).
- [15] M. D. Glinchuk and A. N. Morozovska, *J. Phys.: Condens. Matter* **16**, 3517 (2004).
- [16] D. R. Tilley, *Finite-size effects on phase transitions in ferroelectrics*. in: *Ferroelectric Thin Films*, ed. C. Paz de Araujo, J. F. Scott, and G. W. Teylor (Gordon and Breach, Amsterdam, 1996) 11.
- [17] L.D. Landau and E.M. Lifshits, *Electrodynamics of Continuous Media*, (Butterworth Heinemann, Oxford, 1980).
- [18] R. Kretschmer and K. Binder, *Phys. Rev. B* **20**, 1065 (1976).
- [19] M. D. Glinchuk, E. A. Eliseev, and V. A. Stephanovich, *Physica B* **332**, 356 (2002).
- [20] M. D. Glinchuk and A. N. Morozovska, *Phys. Stat. Sol. (b)* **238**, 81 (2003).
- [21] H. Huang, C. Q. Sun, Zh. Tianshu and P. Hing, *Phys. Rev. B*, **63**, 184112 (2001).
- [22] J. Freund, J. Halbritter, and J. K. H. Horber, *Microsc. Res. Tech.* **44**, 327 (1999).
- [23] J. Zhang, Zh. Yin, M.-Sh. Zhang, and J. F. Scott, *Solid State Communications* **118**, 241 (2001).
- [24] W. Ma, M. Zhang, and Z. Lu, *Phys. Stat. Sol. (a)* **166**, 811 (1998).
- [25] J. S. Speck, W. Pompe, *J. Appl. Phys.* **76**, 466 (1994).
- [26] A. Erdelyi et al. *Higher transcendental functions*. Vol. 2, (New-York, Toronto, London Mc Graw-Hill Book Company, 1953)
- [27] Note, that for RS because of its monoclinic symmetry the coefficient $2Q_{12}$ in Eq.(14) should be substituted with $(Q_{12} + Q_{13})$, which can be found for instance in I. S. Zhelezov, *Electrical crystals* (Nauka, Moscow, 1979) in rus.
- [28] R. Blinc and B. Zeks, *Soft Mode in Ferroelectrics and Antiferroelectrics* (North-Holland Publishing Company, Amsterdam, Oxford, 1974).
- [29] A. I. Lurie, *Spatial problems of the elasticity theory*, (Gos. Izd. Teor. Tekh. Lit., Moscow, 1955) in rus.

Appendix A

The free energy expansion on polarization $\mathbf{P} = (0, 0, P_3)$ and stress σ_i powers has the form [21], [14]:

$$F = a_1 P_3^2 + a_{11} P_3^4 + a_{111} P_3^6 - Q_{11} \sigma_3 P_3^2 - Q_{12} (\sigma_1 + \sigma_2) P_3^2 - \frac{1}{2} s_{11} (\sigma_1^2 + \sigma_2^2 + \sigma_3^2) - s_{12} (\sigma_1 \sigma_2 + \sigma_1 \sigma_3 + \sigma_3 \sigma_2) - \frac{1}{2} s_{44} (\sigma_4^2 + \sigma_5^2 + \sigma_6^2) \quad (\text{A.1})$$

Hereinafter we use Voigt notation σ_i or matrix notation σ_{nm} (xx=1, yy=2, zz=3, zy=4, zx=5, xy=6) when it necessary.

Firstly let us calculate the σ_i components caused by the uniform lateral pressure related to the effective surface tension $p = \mu/R$ [24], [10]. This Lame's problem is discussed in details in [29]. It is easy to obtain that generalized pressure is directed along the cylinder normal, i.e. $\mathbf{p} \uparrow\uparrow \mathbf{n}$. The conditions of mechanical equilibrium $n_i \sigma_{ij} = -p_j$ on the surface of cylindrical solid body have the following form in the cylindrical coordinates (ρ, φ, z) :

$$\sigma_{\rho\rho} \Big|_{\rho=R} = -p, \quad \sigma_{\rho\varphi} \Big|_{\rho=R} = 0, \quad \sigma_{\rho z} \Big|_{\rho=R} = 0, \quad \sigma_{zz} \Big|_{z=\pm h/2} = 0, \quad \sigma_{z\rho} \Big|_{z=\pm h/2} = 0, \quad \sigma_{z\varphi} \Big|_{z=\pm h/2} = 0 \quad (\text{A.2})$$

The conditions of mechanical equilibrium $\partial \sigma_{ij} / \partial x_i = 0$ in the bulk of solid body are the following:

$$\begin{cases} \frac{\partial \sigma_{zz}}{\partial z} + \frac{\partial \sigma_{z\rho}}{\partial \rho} + \frac{\sigma_{z\rho}}{\rho} + \frac{1}{\rho} \frac{\partial \sigma_{z\varphi}}{\partial \varphi} = 0, \\ \frac{\partial \sigma_{\rho\rho}}{\partial \rho} + \frac{\sigma_{\rho\rho} - \sigma_{\varphi\varphi}}{\rho} + \frac{1}{\rho} \frac{\partial \sigma_{\rho\varphi}}{\partial \varphi} + \frac{\partial \sigma_{z\rho}}{\partial z} = 0, \\ \frac{1}{\rho} \frac{\partial \sigma_{\varphi\varphi}}{\partial \varphi} + \frac{\partial \sigma_{z\varphi}}{\partial z} + \frac{\partial \sigma_{\rho\varphi}}{\partial \rho} + 2 \frac{\sigma_{\rho\varphi}}{\rho} = 0. \end{cases} \quad (\text{A.3})$$

It is seen that boundary and equilibrium conditions (A.2) and (A.3) can be fulfilled with

$$\sigma_{\rho\rho} = \sigma_{\varphi\varphi} = -p, \quad \sigma_{\rho\varphi} = 0, \quad \sigma_{\rho z} = 0, \quad \sigma_{zz} = 0, \quad \sigma_{z\varphi} = 0. \quad (\text{A.4})$$

The tensor components in Cartesian coordinates can be found from relations:

$$\begin{pmatrix} \sigma_{xx} & \sigma_{xy} & \sigma_{xz} \\ \sigma_{yx} & \sigma_{yy} & \sigma_{yz} \\ \sigma_{zx} & \sigma_{zy} & \sigma_{zz} \end{pmatrix} = \begin{pmatrix} \cos(\varphi) & -\sin(\varphi) & 0 \\ \sin(\varphi) & \cos(\varphi) & 0 \\ 0 & 0 & 1 \end{pmatrix} \cdot \begin{pmatrix} \sigma_{\rho\rho} & \sigma_{\rho\varphi} & \sigma_{\rho z} \\ \sigma_{\varphi\rho} & \sigma_{\varphi\varphi} & \sigma_{\varphi z} \\ \sigma_{z\rho} & \sigma_{z\varphi} & \sigma_{zz} \end{pmatrix} \cdot \begin{pmatrix} \cos(\varphi) & \sin(\varphi) & 0 \\ -\sin(\varphi) & \cos(\varphi) & 0 \\ 0 & 0 & 1 \end{pmatrix} \quad (\text{A.5})$$

Allowing for Eq. (A.4), expression (A.5) leads to

$$\begin{aligned} \sigma_{xx} &= \cos(\varphi)^2 \sigma_{\rho\rho} + \sin(\varphi)^2 \sigma_{\varphi\varphi} = -p, \\ \sigma_{yy} &= \sin(\varphi)^2 \sigma_{\rho\rho} + \cos(\varphi)^2 \sigma_{\varphi\varphi} = -p, \\ \sigma_{xy} &= \cos(\varphi) \sin(\varphi) (\sigma_{\rho\rho} - \sigma_{\varphi\varphi}) = 0, \\ \sigma_{xz} &= \sigma_{yz} = \sigma_{zz} = 0. \end{aligned} \quad (\text{A.6})$$

In Voigt notation this gives:

$$\sigma_1 = \sigma_2 = -\frac{\mu}{R}, \quad \sigma_3 = \sigma_4 = \sigma_5 = \sigma_6 = 0. \quad (\text{A.7})$$

The anzats of solutions (A.7) into the free energy (A.1) gives the expression:

$$F = \left(a_1 + 2Q_{12} \frac{\mu}{R} \right) P_3^2 + a_{11} P_3^4 + a_{111} P_3^6 - (s_{11} + s_{12}) \frac{\mu^2}{R^2} \quad (\text{A.8})$$

The minimization of free energy (A.8) on the polarization components $\partial F / \partial P_3 = E_0$ gives the equation of state.

Note, that the renormalization of coefficient $a_1^* = (a_1 + 2Q_{12}p)$ for a cylindrical nanoparticle differs from the one $a_1^* = (a_1 + (Q_{11} + 2Q_{12})p)$ obtained for a spherical nanoparticle by [21]. Both results are clear owing to the fact that $\sigma_1 = \sigma_2 = -p$ and $\sigma_3 = 0$ for a cylinder, whereas $\sigma_1 = \sigma_2 = \sigma_3 = -p$ for a sphere. Also let us underline that we do not take into account possible stress relaxation caused by dislocations and disclinations. This approach used by many authors (see e.g. [21], [14], [29]) is valid under the conditions discussed elsewhere [25].

Appendix B

Let us consider the depolarization field distribution for the case of cylindrical particle with arbitrary polarization distribution in the ambient conditions. In the equilibrium the perfect screening can be achieved so that there will be no electric field outside the particle.

The field distribution can be obtained on the basis of the electrostatic Poisson's equation for the electric potential φ :

$$\Delta\varphi(\rho, z) = 4\pi \operatorname{div} \mathbf{P}(\rho, z) \quad (\text{B.1})$$

Here $\mathbf{P}(\rho, z) = (0, 0, P_z)$ is the given z-component polarization distribution inside the particle, which has the cylindrical symmetry: $\Delta = \frac{\partial^2}{\partial z^2} + \frac{1}{\rho} \frac{\partial}{\partial \rho} \rho \frac{\partial}{\partial \rho}$. The boundary conditions on the particle surface has the view:

$$\varphi(\rho = R, z) = 0, \quad \varphi\left(\rho, z = -\frac{h}{2}\right) = 0, \quad \varphi\left(\rho, z = \frac{h}{2}\right) = U. \quad (\text{B.2})$$

Here R and h is the cylinder radius and height respectively, U is the applied voltage. At $U = 0$ the boundary conditions (B.2) corresponds to the short-circuit ones proposed by Kretschmer and Binder [18] for a film.

The system (B.1), (B.2) can be solved by means of the separation of variables method. Since for the system of cylindrical symmetry eigen-functions of Laplace operator Δ are the Bessel functions one can find the potential φ in the form of series:

$$\varphi(\rho, z) = \sum_{n=1}^{\infty} C_n(z) J_0\left(k_n \frac{\rho}{R}\right) \quad (\text{B.3})$$

Here $J_0(x)$ is the first kind Bessel function of zero order, k_n is the n-th root of this function ($J_0(k_n) = 0$) and functions $C_n(z)$ should satisfy the following boundary problem:

$$\begin{cases} \frac{d^2 C_n(z)}{dz^2} - \left(\frac{k_n}{R}\right)^2 C_n(z) = 4\pi \frac{2}{R^2 J_1(k_n)^2} \int_0^R \frac{\partial P_Z(\rho, z)}{\partial z} J_0\left(k_n \frac{\rho}{R}\right) \rho d\rho \\ C_n\left(z = -\frac{h}{2}\right) = 0, \quad C_n\left(z = \frac{h}{2}\right) = \frac{2}{k_n J_1(k_n)} U \end{cases} \quad (\text{B.4})$$

In (B.4) we used the Bessel functions orthogonality $\int_0^R J_0\left(k_n \frac{\rho}{R}\right) J_0\left(k_m \frac{\rho}{R}\right) \rho d\rho = \delta_{nm} \frac{R^2 J_1(k_n)^2}{2}$,

integral $\int_0^R J_0\left(k_n \frac{\rho}{R}\right) \rho d\rho = R^2 \frac{J_1(k_n)}{k_n}$ and expansion $1 = \sum_{n=1}^{\infty} \frac{2}{k_n J_1(k_n)} J_0\left(k_n \frac{\rho}{R}\right)$ at $\rho < R$. In accordance

with the general theory of the linear second order differential equations one can find the solution of (B.4) in the form:

$$\begin{aligned} C_n(z) &= \sum_{m=1}^{\infty} g_{mn} \sin\left(\frac{2\pi m z}{h}\right) + A_n \exp\left(\frac{k_n z}{R}\right) + B_n \exp\left(-\frac{k_n z}{R}\right), \\ g_{mn} &= -\frac{4\pi}{\left(\frac{2\pi m}{h}\right)^2 + \left(\frac{k_n}{R}\right)^2} \int_{-h/2}^{h/2} \frac{2dz}{h} \sin\left(\frac{2\pi m z}{h}\right) \int_0^R \frac{2\rho d\rho}{R^2 J_1(k_n)^2} J_0\left(k_n \frac{\rho}{R}\right) \frac{\partial P_Z(\rho, z)}{\partial z}, \\ A_n &= \frac{2U}{k_n J_1(k_n)} \frac{\exp\left(-\frac{k_n h}{2R}\right)}{1 - \exp\left(-\frac{2k_n h}{R}\right)}, \quad B_n = -\frac{2U}{k_n J_1(k_n)} \frac{\exp\left(-\frac{3k_n h}{2R}\right)}{1 - \exp\left(-\frac{2k_n h}{R}\right)}. \end{aligned} \quad (\text{B.5})$$

Keeping in mind (B.3) and (B.5) one obtains that depolarization field z-component $E_Z^d = -\partial\varphi(\rho, z)/\partial z$ acquires the form after integrating over parts:

$$\begin{aligned} E_Z^d(\rho, z) &= \sum_{m=1}^{\infty} \sum_{n=1}^{\infty} E_{mn} \cos\left(\frac{2\pi m}{h} z\right) J_0\left(k_n \frac{\rho}{R}\right), \\ E_{mn} &= -4\pi \frac{(2\pi m R)^2}{(2\pi m R)^2 + (k_n h)^2} P_{mn}, \\ P_{mn} &= \int_{-h/2}^{h/2} \frac{2d\tilde{z}}{h} \cos\left(\frac{2\pi m}{h} \tilde{z}\right) \int_0^R \frac{2\tilde{\rho} d\tilde{\rho}}{R^2 J_1(k_n)^2} J_0\left(k_n \frac{\tilde{\rho}}{R}\right) P_Z(\tilde{\rho}, \tilde{z}). \end{aligned} \quad (\text{B.6})$$

Note, that coefficients P_{mn} coincide with the ones in polarization expansion:

$$P_Z(\rho, z) = \sum_{m=0}^{\infty} \sum_{n=1}^{\infty} P_{mn} \cos\left(\frac{2\pi m}{h} z\right) J_0\left(k_n \frac{\rho}{R}\right). \quad (\text{B.7})$$

It should be noticed that contrast to (B.6) the expansion (B.7) contains the terms with

$$P_{0n} = \int_{-h/2}^{h/2} \frac{2d\tilde{z}}{h} \int_0^R \frac{2\tilde{\rho}d\tilde{\rho}}{R^2 J_1(k_n)^2} J_0\left(k_n \frac{\tilde{\rho}}{R}\right) P_Z(\tilde{\rho}, \tilde{z}) \quad \text{related to the average polarization}$$

$$\langle P_Z(\rho, z) \rangle = \sum_{n=1}^{\infty} P_{0n} \frac{2J_1(k_n)}{k_n}. \quad \text{The difference } P_Z(\rho, z) - \langle P_Z(\rho, z) \rangle \text{ acquires the form:}$$

$$P_Z(\rho, z) - \langle P_Z(\rho, z) \rangle = \sum_{m=1}^{\infty} \sum_{n=1}^{\infty} P_{mn} \cos\left(\frac{2\pi m}{h} z\right) J_0\left(k_n \frac{\rho}{R}\right) + \sum_{n=1}^{\infty} \left(J_0\left(k_n \frac{\rho}{R}\right) - \frac{2J_1(k_n)}{k_n} \right) P_{0n} \quad (\text{B.8})$$

Let us assume the good convergence of the series in (B.7)-(B.8) and consider the particular following cases.

1) In the particular case $h \ll \pi R$ one obtains that $\frac{1}{1 + (k_n h / 2\pi m R)^2} \approx 1$ at $n \leq m$ and

$$P_{mn} \approx \frac{2}{k_n J_1(k_n)} \int_{-h/2}^{h/2} \frac{2d\tilde{z}}{h} \cos\left(\frac{2\pi m}{h} \tilde{z}\right) P_Z(0, \tilde{z}) \quad \text{in accordance with Laplace method. Then we derive that}$$

$$\text{the term } \sum_{n=1}^{\infty} \left(J_0\left(k_n \frac{\rho}{R}\right) - \frac{2J_1(k_n)}{k_n} \right) P_{0n} = 0 \quad \text{allowing for the unity expansion } 1 = \sum_{n=1}^{\infty} \frac{2}{k_n J_1(k_n)} J_0\left(k_n \frac{\rho}{R}\right)$$

$$\text{and equalities } 1 \equiv \sum_{n=1}^{\infty} \frac{4}{k_n^2} \equiv \sum_{n=1}^{\infty} \frac{2}{k_n J_1(k_n)}, \text{ which can be easily obtained from the unity expansion. Thus}$$

the approximate expression for depolarization field has the form (see (B.6)-(B.8)):

$$E_Z^d(z) \approx -4\pi(P_Z(z) - \langle P_Z(z) \rangle) \quad (\text{B.9})$$

Note, that (B.9) is exact at $R \rightarrow \infty$ and coincides with the one obtained in [18] at $P_Z(\rho, z) \equiv P_Z(z)$.

2) In the particular case $h \gg \pi R$ one obtains that $\frac{1}{1 + (k_n h / 2\pi m R)^2} \approx \left(\frac{2R}{h}\right)^2$ at $n \leq m$. Thus the

depolarization field is rather small in comparison with (B.9), namely:

$$|E_Z^d(\rho, z)| \sim 4\pi \left(\frac{2R}{h}\right)^2 (P_Z(z) - \langle P_Z(z) \rangle). \quad (\text{B.10})$$

The interpolation for the depolarization field that contains the aforementioned particular cases (B.9)-(B.10) acquires the form:

$$E_Z^d(\rho, z) = -\frac{4\pi}{1 + (h/2R)^2} (P_Z(z) - \langle P_Z(z) \rangle) \quad (\text{B.11})$$